Petroleum Science 23 (2026) 1445–1458

Contents lists available at ScienceDirect

Petroleum Science

journal homepage: www.keaipublishing.com/en/journals/petroleum-science

Original Paper

Pore scale phase behavior of condensate gas in porous media: Insights from 2D NMR T_1–T_2 spectrum method

Yi-Sheng Hu [a,*], Heng Wang [a], Ping Guo [a,**], Yang Zhao [a,b]

[a] Petroleum Engineering School, Southwest Petroleum University, Chengdu, 610500, Sichuan, China
[b] The 4th Oil Production Plant of Changqing Oilfield Company, PetroChina, Yulin, 718500, Shaanxi, China

ARTICLE INFO

Article history:
Received 17 June 2025
Received in revised form
31 October 2025
Accepted 3 November 2025
Available online 20 November 2025

Edited by Yan-Hua Sun

Keywords:
2D NMR
Nanoscale confinement
Phase behavior
Condensate gas
Pressure/volume/temperature (PVT)

ABSTRACT

The widespread development of unconventional oil and gas reservoirs has advanced reservoir research to the nanoscale level. Under the influence of nanoscale confinement effects, the phase behavior of condensate gas reservoirs deviates from the classical theories derived from traditional pressure/volume/temperature (PVT) experiments. Therefore, studying the phase behavior of fluids in porous media at the nanoscale is significant. The experiment employs two-dimensional nuclear magnetic resonance T_1–T_2 (2D NMR T_1–T_2) spectrum method to study the phase behavior characteristics of condensate gas in three cores with varying degrees of tightness, then explores the effects of different cores and different CO_2 contents on the phase behavior characteristics of condensate gas. As the core tight degrees of cores increases, the dew point pressure rises from 25.9 to 27.9 MPa while restricting fluid migration within the pores. The maximum condensate oil saturation increases from 10.35% to 17.35%. Compared with the bulk PVT phase experiment, the dew point pressure of condensate gas in porous media is lower than that of condensate gas in the PVT visualization cell. This is related to the formation of phase mixing and "liquid bridges" when oil and gas reach the dew point pressure in porous media. The retrograde condensation phenomenon in condensate gas systems in different porous media occurs first in the micropores. CO_2 inhibits the retrograde condensation phenomenon in tight cores, and CO_2 concentration is negatively correlated with the dew point pressure of the condensate gas.

1. Introduction

Due to their vast geological reserves and high economic value, the extensive development of condensate gas reservoirs occupies an important position in the global exploration and utilization of oil and gas resources (Arias-Ortiz and Patzek, 2025; Dorhjie et al., 2025; Liu Y. et al., 2025). However, the exploitation of condensate gas reservoirs faces unique challenges, primarily due to their dual oil and gas characteristics and complex phase changes (Liu Y. et al., 2025; Meng and Sheng, 2016; Tang et al., 2021). When the formation pressure drops below the dew point pressure, the heavier components precipitate in liquid form, forming a gas–liquid two-phase flow, significantly increasing exploitation's difficulty. Additionally, the nanoscale complex pore structures in unconventional reservoirs more easily lead to the adsorption of heavy components, and the damage caused by condensate oil severely reduces recovery efficiency (Amani and Nguyen, 2015; Long et al., 2024; Rabiei et al., 2015; Shi et al., 2015). Therefore, explaining the phase behavior characteristics and compositional changes of condensate gas in porous media is a significant challenge for researchers.

For a long time, the development of condensate gas reservoirs has been based on phase behavior results summarized from PVT experiments, with bulk PVT phase behavior being the most commonly studied, usually without considering the influence of porous media (Li A. et al., 2024; Luo et al., 2021; Sun et al., 2012; Tuo et al., 2024). However, under actual reservoir conditions, the effect of porous media on phase characteristics of condensate gas is significant (Dorhjie et al., 2024; Jing et al., 2024; Liu et al., 2024; Suleimanov et al., 2018). Researchers have developed many experimental methods to study the phase behavior of

* Corresponding author.
** Corresponding author.
E-mail addresses: yisheng.hu@swpu.edu.cn (Y.-S. Hu), guopingswpi@vip.sina.com (P. Guo).
Peer review under the responsibility of China University of Petroleum (Beijing).

https://doi.org/10.1016/j.petsci.2025.11.007

hydrocarbons in oil and gas reservoirs based on porous media, for example, phase studies in PVT cells filled with quartz sand and clay minerals, simulating porous media using fine tubes filled with quartz sand, or conducting long core depletion experiments using field cores (Jing et al., 2024a; Li et al., 2013; Lu et al., 2024; Zhang et al., 2021), and determining condensate gas phase changes by detecting the composition of the produced fluids with a gas chromatograph (Jing et al., 2023, Jing et al., 2024b; Wang P. et al., 2025). Alternatively, microfluidic chips can be used to directly observe the phase characteristics of condensate gas in different pore and throat regions (Dawaymeh et al., 2025). However, regardless of whether porous media are filled in PVT cells, fine tubes, or long core experiments, these methods rely on repeated chromatographic analysis of the products, which can only determine the onset of retrograde condensation of condensate gas in porous media. Quantitative analysis of condensate liquid saturation during retrograde condensation in porous media still lacks research. Moreover, the manufacturing cost of microfluidic chips is high, and precise pressure and temperature control are required to prevent damage to the chips due to varying conditions. Hence, establishing a cost-effective experimental method to quantify the phase behavior of condensate gas in porous media is an urgent priority.

Nuclear magnetic resonance (NMR) method plays a significant role in the petroleum and natural gas industry, being widely used to evaluate reservoir characteristics and productivity, analyze hydrogen-containing substances such as water and hydrocarbons in reservoirs, and accurately measure conventional reservoir properties (Aliyev et al., 2016; Chai et al., 2022; Hassan et al., 2020; Wang X. et al. 2023; Wang S. et al., 2024b). Typically, NMR testing includes one-dimensional (1D NMR) and two-dimensional (2D NMR) techniques. 1D NMR tests either longitudinal relaxation time T_1 or transverse relaxation time T_2, while 2D NMR examines both T_1 and T_2 indicators simultaneously (Hu et al., 2012; Li et al., 2024; Li et al., 2022). When oil, gas, and water coexist in the pores, the T_2 spectral signals overlap, so 2D NMR T_1–T_2 spectrum method shows clear technical advantages in distinguishing hydrogen-containing solid components, identifying fluid types in fine pores, and describing pore structure details (Alanazi et al., 2023; Gu et al., 2023; Li X. et al., 2024; Xu et al., 2024; Zhang et al., 2024). Liu et al. (2022) used 2D NMR T_1–T_2 spectrum method to intuitively show water, oil, bound water, solid organic matter in shale, and the oil–water migration process in the pores. Sun and Guo (2022) distinguished the NMR signals of condensate oil and condensate gas in cores using the T_1/T_2 ratio and peak signal differences, believing condensate oil primarily forms in small pores and retrograde condensation mainly occurs in medium and large pores. Wang X. et al. (2023) used 2D NMR T_1–T_2 spectrum method to demonstrate that shale oil exists in different phases in pores of varying sizes and exhibits different flow properties. Wang J. et al. (2024) studied fluid phase behavior in shale using 2D NMR T_1–T_2 spectrum method, delineating the distribution of bound water, adsorbed oil, bound oil, and movable oil under different pore sizes, and concluded that the presence of water altered the phase characteristics of the oil. Dianshi et al. (2024) observed using 2D NMR T_1–T_2 spectrum method that shale oil only begins to move when it reaches the movable threshold, and that microfractures enhance the oil's mobility. In contrast, adsorbed oil impedes its movement in the pores. Li C. et al. (2024) used 2D NMR T_1–T_2 spectrum method to identify five types of fluid components, including clay-bound water, capillary-bound water, free water, bound oil, and free oil and calculated their volumes. Wang J. et al. (2025) established a method for the quantitative evaluation of oil and water contents in shale using 2D NMR T_1–T_2 spectrum method, verifying the results with MRE pyrolysis. Zou et al. (2024) explored the effect of CO_2 on the oil phase using T_1–T_2 spectrum and found that high-pressure CO_2 injection promotes the migration of free oil from large pores to small pores and leads to more oil being adsorbed. Although the 2D NMR T_1–T_2 spectrum method has been widely applied in studies of fluid composition, distribution, and pore characteristics, research on changes in fluid phase behavior remains limited. This is especially true for fluids like condensate gas, whose phase behavior characteristics are influenced by multiple factors such as pore features, pressure, and temperature, thus necessitating efficient, concise, and high-precision research methods.

Considering the impact of porous media, this study establishes a novel method for determining condensate gas phase behavior characteristics. The research investigates changes in condensate gas phase behavior characteristics in cores with different nanoscale pore sizes and the effect of CO_2 on these changes. The experiment utilizes in-situ real time NMR scanning to obtain 2D NMR T_1–T_2 spectrum. Based on these spectra, the condensate oil

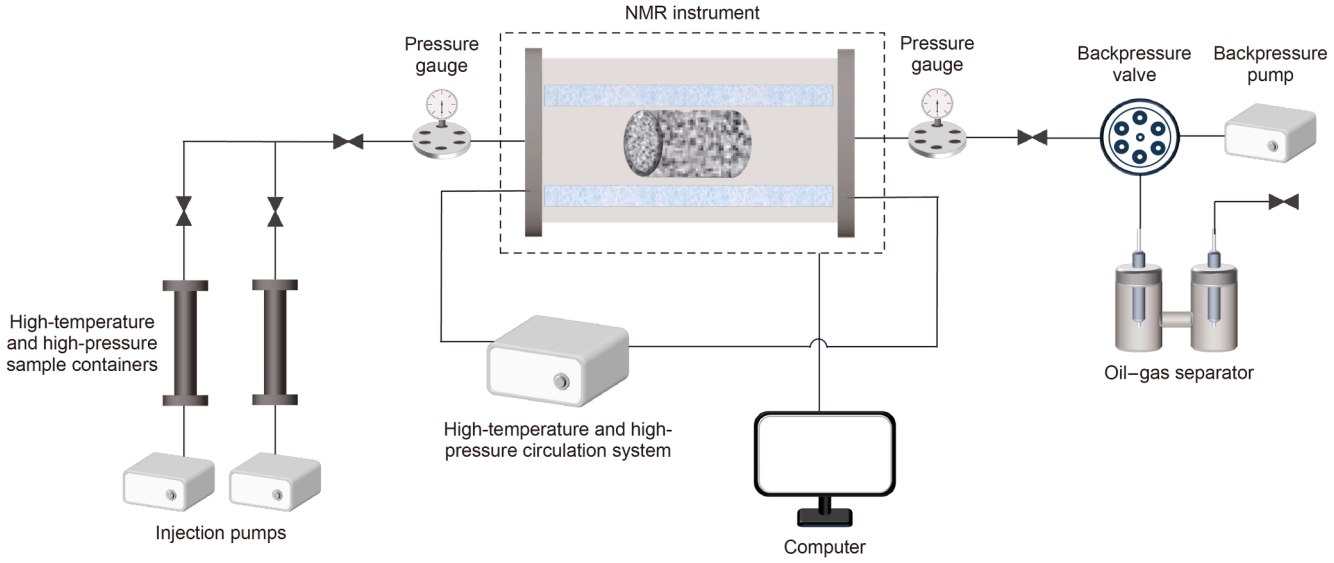

Fig. 1. The in-situ, real-time 2D NMR equipment used to aquire T_1–T_2 spectra.

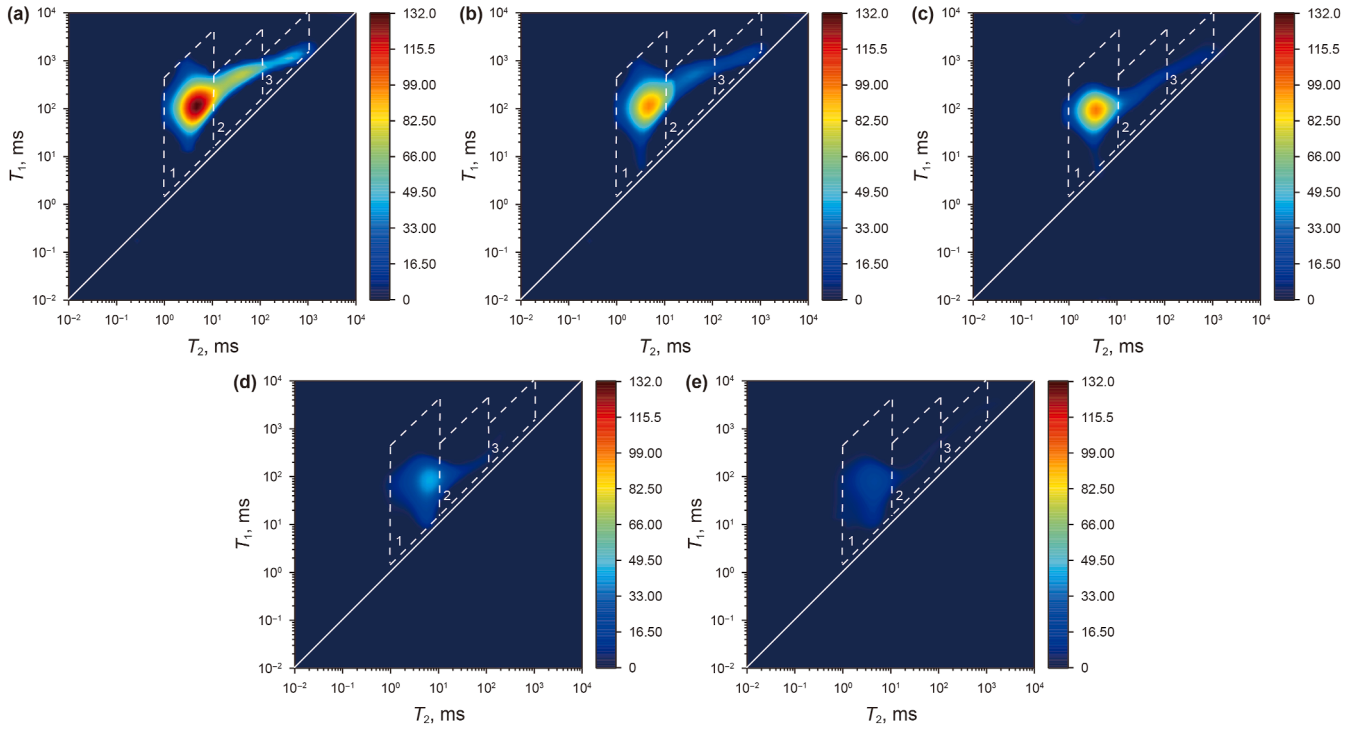

Fig. 2. 2D NMR T_1–T_2 standard spectra of condensate oil in core 1#, describing the distribution of condensate oil at saturation of 100% (**a**), 74.15% (**b**), 52.44% (**c**), 31.00% (**d**), and 22.57% (**e**), respectively. The diagonal line with a slope of 1 in the middle represents the T_1/T_2 iso-line, and the white dashed rhombus frames indicate the signal range for different pore regions. The color scale on the right shows the hydrogen signal intensity at specified T_1 and T_2 coordinates.

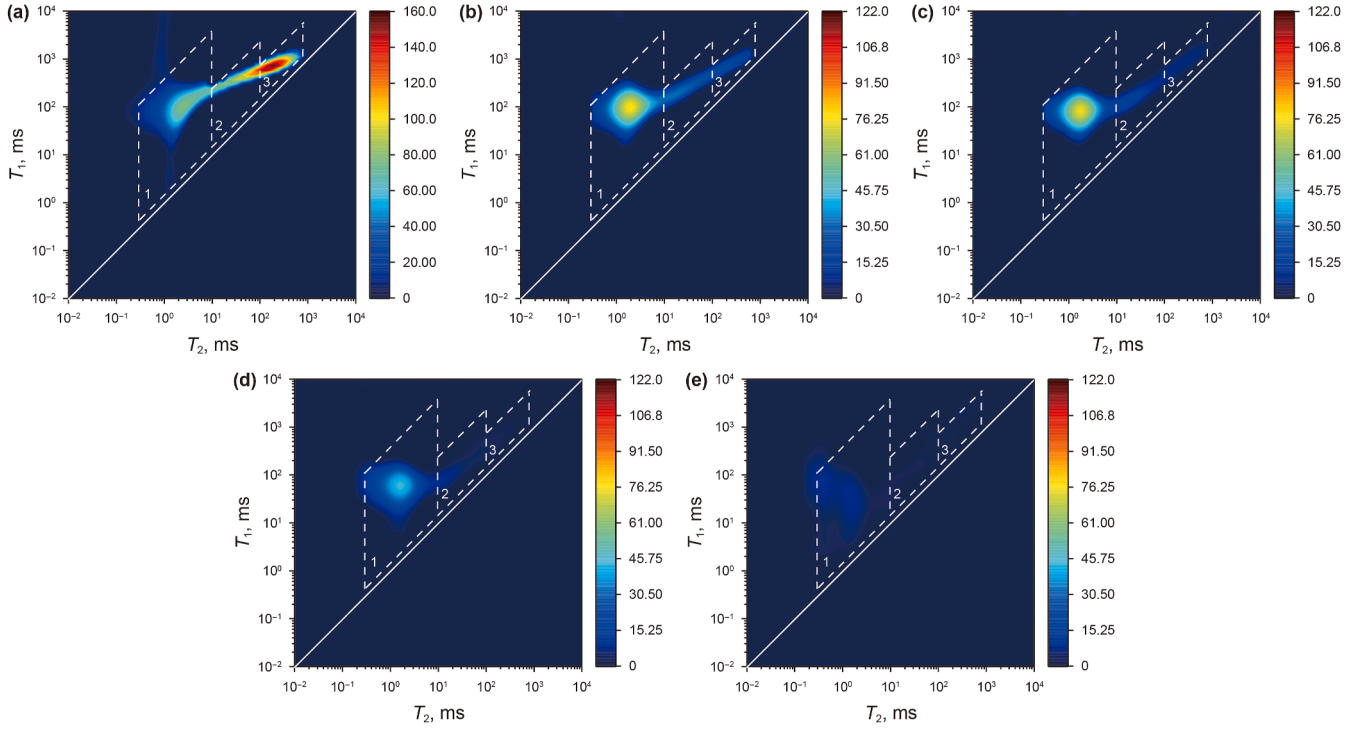

Fig. 3. 2D NMR T_1–T_2 standard spectra of condensate oil in core 2#, describing the distribution of condensate oil at saturation of 100% (**a**), 64.50% (**b**), 51.28% (**c**), 34.68% (**d**), and 14.58% (**e**), respectively. The diagonal line with a slope of 1 in the middle represents the T_1/T_2 iso-line, and the white dashed rhombus frames indicate the signal range for different pore regions. The color scale on the right shows the hydrogen signal intensity at specified T_1 and T_2 coordinates.

identification maps during the pressure depletion process are analyzed under varying core properties and CO_2 contents. The condensate oil saturation in each region is calculated to clarify the phase behavior characteristics of condensate gas under nanoscale confinement, considering the influence of porous media properties and CO_2 content. The experimental results are then compared and analyzed against those obtained from bulk PVT phase measurements.

2. Methodology

2.1. Materials

In this experiment, the condensate gas sample was reconstituted by dry gas, condensate oil, and *n*-heptane (purity 99.97%, analytical grade, Chengdu Kelong Chemicals Co., Ltd., China) in a ratio of 90:5:5. The addition of *n*-heptane aims to lower the dew point pressure of the prepared condensate gas, ensuring that the depletion experiment of the condensate gas in the core can be successfully conducted in the core displacement experiment using the in-situ real time NMR scanning experimental apparatus. The maximum pressure and temperature of the apparatus are 40 MPa and 100 °C, respectively. The specific composition of the condensate gas sample was shown in Table S1 and Fig. S1 of the supporting information.

To investigate the impact of pore structure on condensate gas phase behavior, three cores were selected based on their porosity, permeability, and pore structures, as well as high-pressure mercury injection tests (AutoPore IV 9505 porosimeter, in Canada). Core 1# had a porosity of 19.76%, a permeability of 12.8 mD, and an average pore-throat radius of 3.109 μm. The corresponding values for cores 2# and 3# were 12.21%, 0.3 mD, 0.673 μm and 10.19%, 0.014 mD, 0.099 μm, respectively. The specific physical parameters of these cores are shown in Table S2 and Fig. S2 of the supporting information.

To study the impact of CO_2 content in the condensate gas on the phase behavior of the condensate gas, different condensate gas samples with different proportions of CO_2 were reconstituted and prepared for the following experiments. The specific CO_2 contents were shown in Table S3 of the supporting information.

2.2. Determination of the phase behavior characteristics of condensate gas systems

In conventional bulk PVT phase experiments, the dew point pressure of condensate gas is typically determined through constant component expansion (CCE) experiments (Li et al., 2017; Tuo et al., 2024; Yao et al., 2016). The bulk PVT phase experiment for condensate gas was conducted using the JEFRI high-temperature and high-pressure reservoir fluid analyzer (Donald Baker Robinson Co., Ltd., Canada). The condensate gas sample was charged into a visualization cell of the JEFRI high-temperature and high-pressure reservoir fluid analyzer. The operating pressure was elevated to 30 MPa, and the system temperature was raised to 80 °C. The system was then maintained under isothermal conditions for 4–5 h, during which continuous mechanical agitation was applied to ensure equilibrium. Subsequently, the pressure was gradually reduced in 2 MPa increments, with each pressure stage maintained for 0.5 h to allow stable system. During this process, the pressure and corresponding gas volume were systematically recorded. The dew point pressure was identified when a small liquid phase first appeared in the visualization cell. To ensure accuracy, the system was re-pressurized to 30 MPa, and the above procedure was repeated three times to obtain a precise measurement of the dew point pressure.

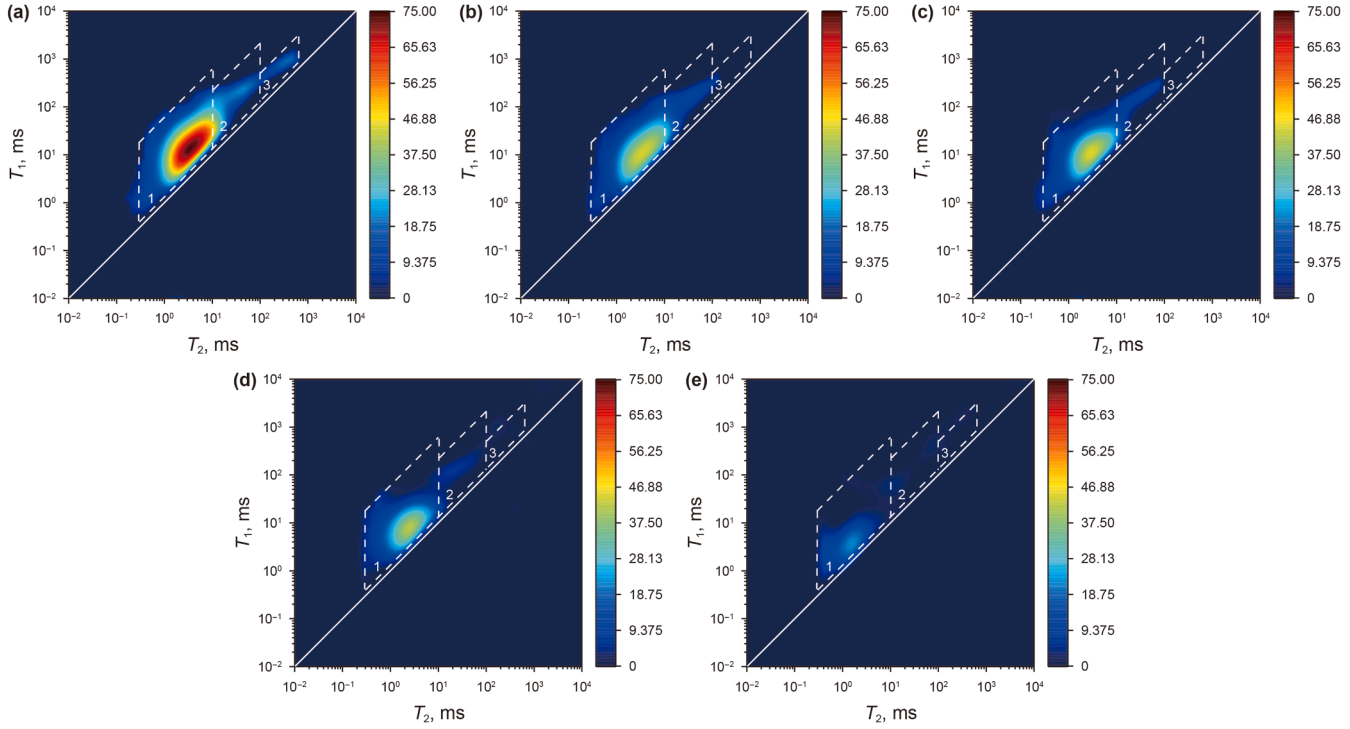

Fig. 4. 2D NMR T_1–T_2 standard spectra of condensate oil in core 3#, describing the distribution of condensate oil at saturation of 100% (**a**), 60.00% (**b**), 48.59% (**c**), 37.80% (**d**), and 18.00% (**e**), respectively. The diagonal line with a slope of 1 in the middle represents the T_1/T_2 iso-line, and the white dashed rhombus frames indicate the signal range for different pore regions. The color scale on the right shows the hydrogen signal intensity at specified T_1 and T_2 coordinates.

Following the determination of the dew point pressure, the pressure was stabilized at the measured dew point pressure for 1 h. The gas volume within the visualization cell was recorded, and a constant-volume depletion experiment was initiated. The pressure was gradually reduced, with the system agitated for 1 h and stabilized for 0.5 h at each stage. The pressure, sample volume, and liquid volume were meticulously recorded at each step. When the system had stabilized, the visualization cell valve was opened to maintain constant pressure while allowing the gas to vent until the sample volume returned to the previously established constant volume. The volume of the liquid phase was recorded, and the pressure was further reduced while maintaining constant volume conditions. This process was continued until the completion of the constant-volume depletion experiment.

2.3. Determination of condensate oil 2D NMR T_1–T_2 standard spectrum

When studying the phase behavior characteristics of condensate gas using 2D NMR T_1–T_2 spectral analysis, it is necessary to determine the standard spectra of condensate oil to define the measurement range (Sun and Guo, 2022). The in-situ real time NMR scanning equipment used in this experiment was the MesoMR12-060H-I NMR analyzer (Suzhou Niumag Co., Ltd., China). The entire experimental setup also included a high-temperature and high-pressure sample container, a high-temperature and high-pressure circulation system, and a core holder (all in Chengdu Qianqu Oil Technology Co., Ltd., China). The high-temperature circulation system used a fluorinated liquid as the pressure transfer medium to provide confining pressure and formation temperature for the core, and the fluorinated liquid did not produce any NMR signal characteristics. During the experiment, N_2 was injected to control the saturation of the condensate oil. A flow chart of the experimental setup can be specified in Fig. 1.

First, the core was soaked and cleaned with petroleum ether (Chengdu Kelong Co., Ltd., China) to remove any surface impurities. The core was then heat-treated at 140 °C for 24 h to eliminate bound water and other hydrogen-containing substances. This thermal treatment continued until no significant NMR signal was detectable in the 2D NMR T_1–T_2 spectrum, ensuring the core was

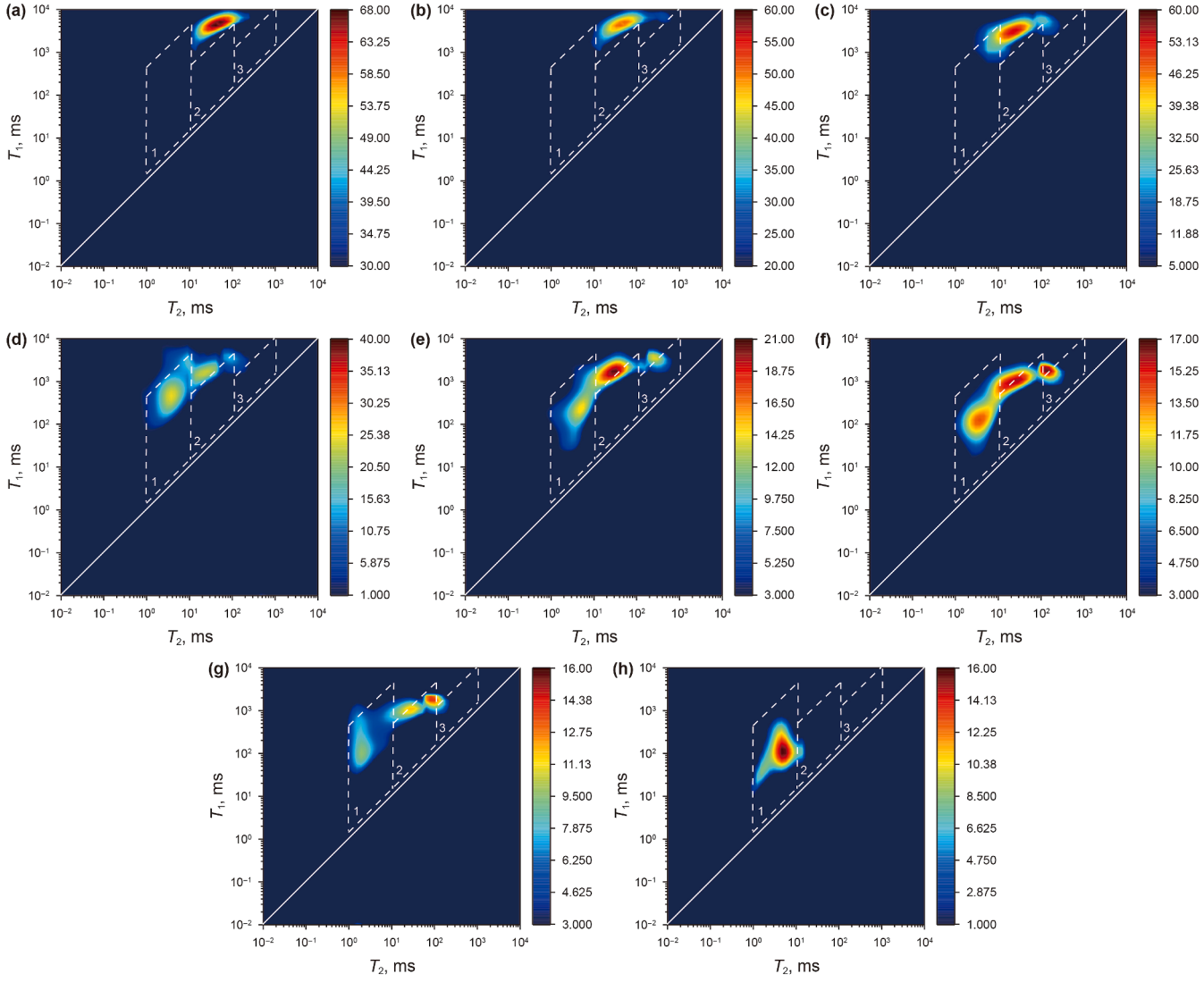

Fig. 5. The 2D NMR T_1–T_2 standard spectra describing the phase behavior of condensate gas in core 1#. (**a**)–(**h**) represent the signal distribution of condensate oil at pressures of 30.0, 25.9, 25.0, 20.0, 13.4, 8.4, 3.4, and 1.0 MPa, respectively. The white dashed rhombus frames indicate the calibrated signal range of condensate oil. The color scale on the right represents the hydrogen signal intensity at specified T_1 and T_2 coordinates.

properly prepared for the subsequent saturation process. In preparation for saturation, the core was placed in the high-temperature and high-pressure sample container, and a vacuum was applied to remove any remaining air. Condensate oil was then pumped into the container to fully saturate the core. The pressure was gradually increased in a stepwise manner, with a pressure gradient of 5 MPa applied at each stage. Each pressure gradient was maintained for 5 h until the final pressure of 30 MPa was reached, marking the completion of the core saturation process.

The fully saturated core was carefully placed in the core holder, with the confining pressure maintained 5 MPa above the inlet pressure to establish a displacement pressure gradient up to 30 MPa. The experiment was conducted at a controlled temperature of 80 °C. Condensate oil was continuously pumped into the core to compensate for losses until the oil flow rate stabilized at the outlet. At this point, the NMR scanning was conducted to analyze the core's initial state. Subsequently, the N_2 injection rate was adjusted to initiate the gas displacement experiment of the condensate oil. Once a specific volume of condensate oil had been displaced, another NMR scanning was performed to calculate the T_1/T_2 ratio. Simultaneously, condensate oil was collected at the outlet to determine the remaining condensate oil saturation in the core.

2.4. In-situ real time NMR scanning experiment for condensate gas

The experiment was designed to determine the 2D NMR T_1–T_2 spectrum of condensate gas phase behavior through in-situ real-time NMR scanning, and to investigate the phase behavior characteristics of condensate gas under different core samples and different CO_2 contents. Following pretreatment, the core samples were placed into the core holder. The system was then heated to a temperature of 80 °C, and the pressure was elevated to 30 MPa using N_2. After reaching equilibrium, condensate gas was injected into the core to achieve full saturation. Subsequently, the outlet valve was adjusted to gradually reduce the pressure at a rate of 2 MPa/h, with a pressure drop gradient of 1 MPa, until the desired pressure was attained. Once the system stabilized, an NMR scanning was conducted for data acquisition, and the T_1/T_2 ratio and condensate oil saturation were computed for analysis.

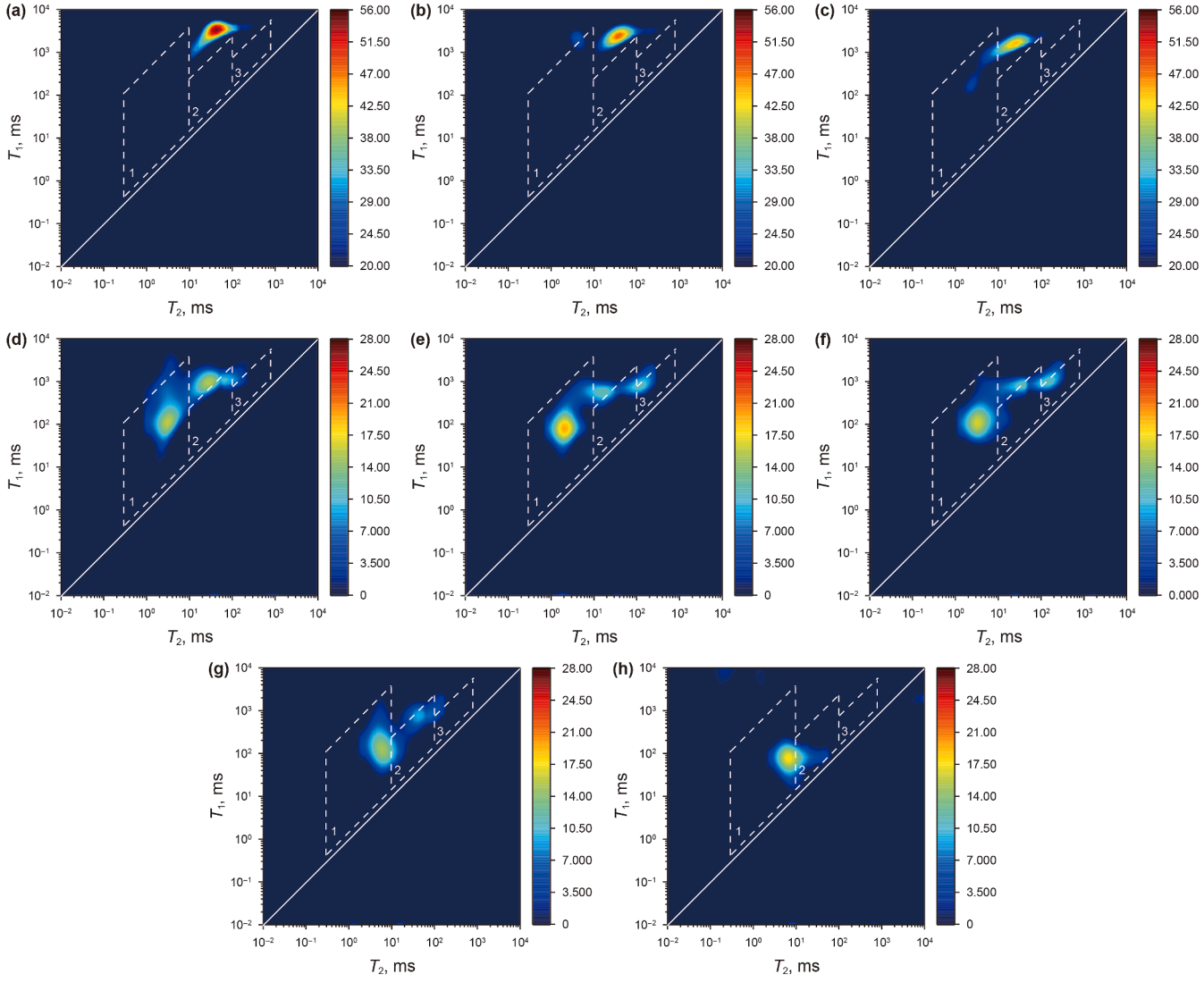

Fig. 6. The 2D NMR T_1–T_2 standard spectra describing the phase behavior of condensate gas in core 2#. (**a**)–(**h**) represent the signal distribution of condensate oil at pressures of 30.0, 26.7, 25.0, 20.0, 15.8, 10.8, 5.8, and 1.0 MPa, respectively. The white dashed rhombus frames indicate the calibrated signal range of condensate oil. The color scale on the right represents the hydrogen signal intensity at specified T_1 and T_2 coordinates.

3. Results and discussion

3.1. Condensate oil 2D NMR T_1–T_2 standard spectrum

The 2D NMR T_1–T_2 standard spectrum of condensate oil is established to delineate its characteristic signal range within the spectrum. The signal range is determined through condensate oil in three core samples with different tight degrees. Figs. 2–4 show the 2D NMR T_1–T_2 standard spectra of condensate oil in cores 1#, 2#, and 3#, respectively. The T_1/T_2 ratio can be used to determine the state of different substances within porous media, and it is necessary to calibrate the corresponding threshold values through NMR scans of reference materials (Kleinberg et al., 1993; Li J. et al., 2018, 2020). According to previous studies, the T_2 relaxation time increases with pore size. By correlating T_2 relaxation data with mercury intrusion porosimetry measurements, the pore structure within cores can be classified into three intervals: micropores ($T_2 < 10$ ms), mesopores (10 ms $< T_2 <$ 100 ms), and macropores ($T_2 > 100$ ms) (Li M. et al., 2020; Sun and Guo, 2022). From Fig. 2, it can be seen in core 1#, the 2D NMR T_2 signal range for condensate oil varies from 0.83 to 1176 ms, with the T_1/T_2 ratio ranging from 1.50 to 389.41, and the peak value at the maximum hydrogen signal occurs at a ratio of 22. The T_1/T_2 recognition values for condensate oil in the micropores, mesopores, and macropores are 389.41, 55.5, and 10, respectively. When the condensate oil saturation is 100%, due to the dispersed pore size distribution of the core, distinct signals are detected in all three regions. The strongest signals from condensate oil are found in the micropores, with some radiation extending into the mesopores and macropores. As the condensate oil saturation decreases to 22.57%, the condensate oil signals in the micropores, mesopores, and macropores gradually weaken. Eventually, signals are only detected in the micropores, with trace signals in the mesopores.

Fig. 3 shows that the T_1/T_2 recognition values for condensate oil in the micropores, mesopores, and macropores are 389.41, 25, and 7.66, respectively. When the condensate oil saturation is 100%, the strongest signals are found in the macropores, radiating to the micropores and mesopores. As the condensate oil saturation decreases, the signal migrates toward the micropores, and eventually, signals from condensate oil are only detected in the

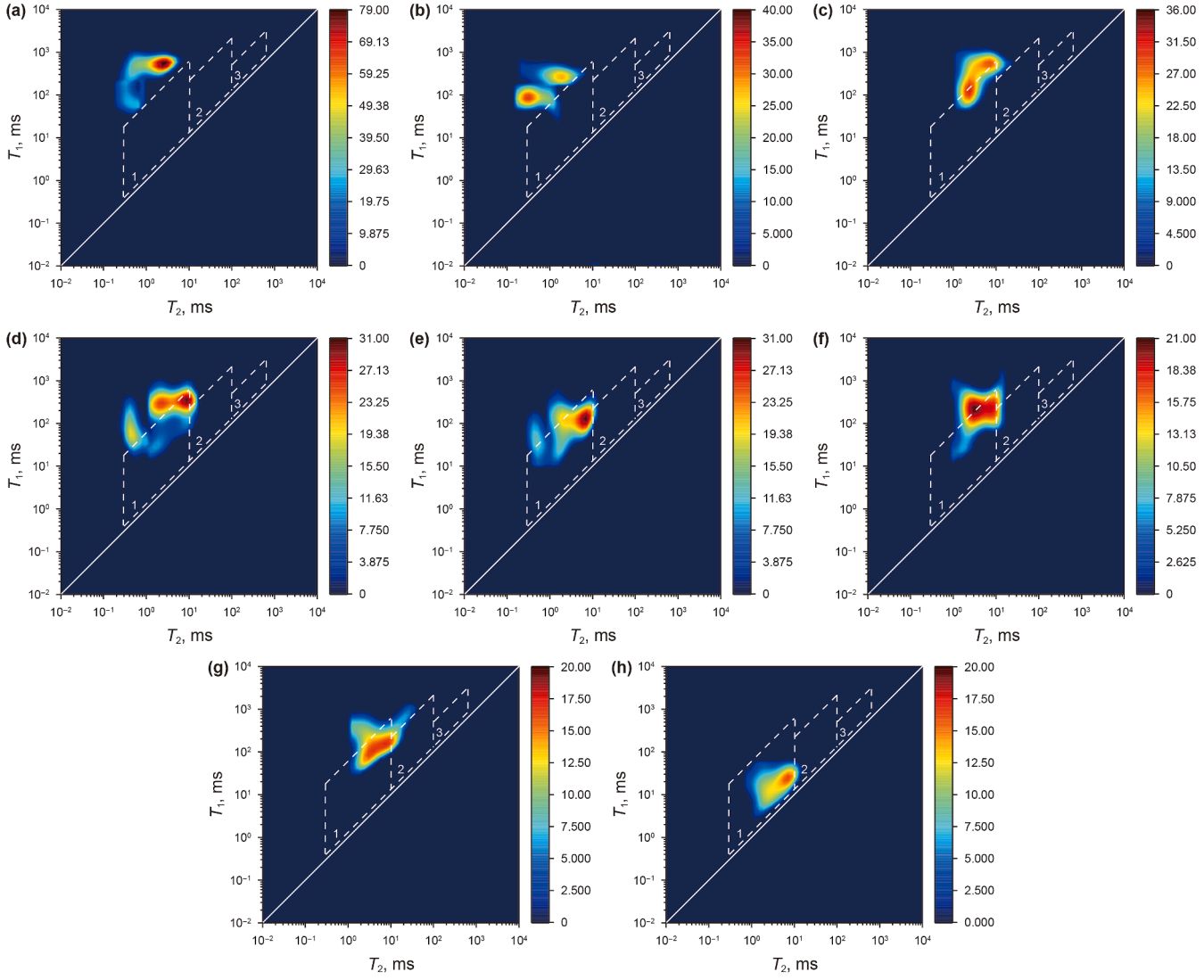

Fig. 7. The 2D NMR T_1–T_2 standard spectra describing the phase behavior of condensate gas in core 3#. (**a**)–(**h**) represent the signal distribution of condensate oil at pressures of 30.0, 27.9, 24.9, 18.7, 13.7, 8.7, 3.7, and 1.0 MPa, respectively. The white dashed rhombus frames indicate the calibrated signal range of condensate oil. The color scale on the right represents the hydrogen signal intensity at specified T_1 and T_2 coordinates.

micropores. Compared to core 1#, the tightness of core 2# increases, with a larger specific surface area, resulting in a shorter longitudinal T_1 relaxation time and a lower T_1/T_2 ratio.

In core 3#, the 2D NMR T_1/T_2 standard spectra of condensate oil are provided in Fig. 4. It can be seen from Fig. 4 that because the pore size distribution in core 3# is more concentrated compared to the previous two cores, the condensate oil signal is also more concentrated, mainly in the micropores, with partial signals detected in the mesopores and macropores. The T_1/T_2 recognition values for condensate oil in the micropores, mesopores, and macropores are 61.5, 25, and 5, respectively. Due to the highest tightness of core 3#, with a permeability of 0.014 mD, it has the largest specific surface area, especially in the micropores, resulting in the lowest upper limit for T_1/T_2 recognition.

Subsequently, the condensate oil saturation in the three core samples was used as the *Y*-coordinate, and the corresponding 2D NMR signal quantity as the *X*-coordinate (Table S4) to study the relationship between them. The results are shown in Fig. S3. The condensate oil saturation and the 2D NMR signal quantity exhibit a linear positive correlation. Through fitting, the correlation coefficients between the condensate oil saturation and the 2D NMR signal quantity for cores 1#, 2#, and 3# are 0.9996, 0.9995, and 0.9991, respectively. This indicates a strong correlation and condensate oil saturation can be calculated using the 2D NMR signal quantity.

3.2. The variation of condensate gas phase behavior in different cores

In core samples, the nature of the fluid changes due to the influence of different porous media (Wan and Mu, 2018). In the experiment, the changes in the phase behavior of condensate gas are studied using 2D NMR T_1–T_2 spectra in three cores with different tight degrees. The experimental results for cores #1, #2, and #3 are shown in Figs. 5–7. The condensate oil saturation in different pore regions is calculated (Fig. S4), and the results were compared with the bulk PVT phase. (Fig. 8). At a pressure of 30 MPa, no condensate oil signal is observed in any of the three cores, indicating that the gas phase was present in all the cores. When the pressure decreased to 27.9 MPa, condensate oil signals first occurred in the micropores of core 3#. As the pressure continued to decrease, the condensate oil in core 3# is mainly concentrated in the micropores (Fig. 7 and Fig. S4(c)). Figs. 5 and 6 show that the dew point pressures for condensate gas in cores 1# and 2# are 25.9 and 26.7 MPa, respectively. Condensate oil signals first occurred in the micropores, followed by the mesopores and macropores. As the pressure continued to deplete, the rate of increase in condensate oil saturation in the micropores is faster than in the mesopores and macropores.

The analysis suggests that condensate oil appears in the micropores earlier because the micropores have a lower pore diameter, forming a curved liquid surface. Under constant temperature, the gas phase has not reached saturation relative to the flat liquid surface. However, it has already reached a supersaturated state in the micropore or capillary, leading to capillary condensation, which increases the dew point pressure (Gallego-Gómez et al., 2018; Salahshoor and Fahes, 2020). Similarly, researchers, who employed microfluidic and computed tomography (CT) scanning experiments to study the impact of pore size on the dew point pressure of condensate gas, observed that

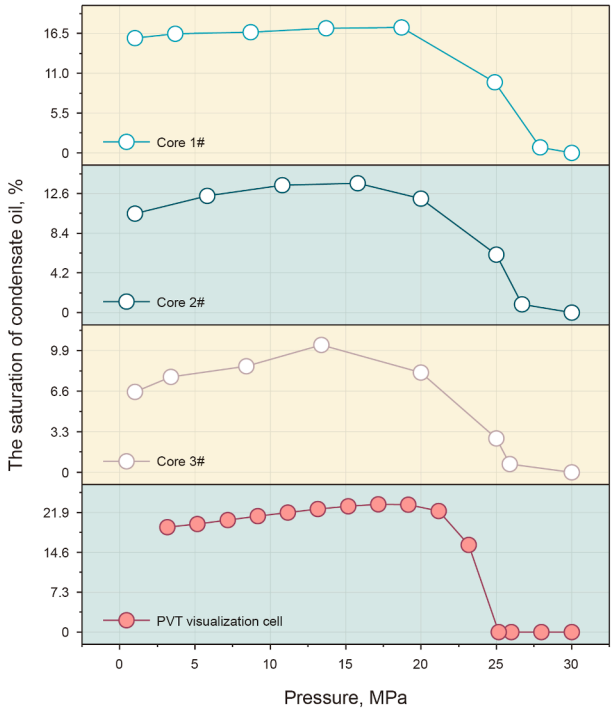

Fig. 8. A comparison of the saturation of condensate oil in the PVT visualization cell and the porous medium. The solid circles represent the results obtained from phase experiments using a PVT visualization cell, while the hollow circles represent the results from the 2D NMR T_1–T_2 spectrum calculation of core samples.

reducing the pore size led to an increase in dew point pressure (Jing et al., 2024b). When the pressure decreases to 15.8 MPa, the overall condensate oil saturation in core 2#, as well as in the micropores and mesopores, reached its maximum, with values of 13.69%, 7.69%, and 4.76%, respectively (Fig. S4). At 10.8 MPa, the macropores reached its maximum condensate oil saturation of 1.65%. At 20 MPa, the micropores in core 1# reached a maximum condensate oil saturation of 5.83%. As the pressure continued to deplete to 13.4 MPa, the overall condensate oil saturation in core 1# reached its maximum value of 10.35%, with the mesopores and macropores achieving maximum condensate oil saturation of 2.79% and 1.73%, respectively. As the pressure continued to deplete, the condensate oil signals in the core shift toward the micropores.

When the system pressure decreased to 1 MPa, the overall condensate oil saturation in cores 1#, 2#, and 3# were 6.54%, 10.45%, and 15.85%, respectively, with condensate oil signals observed in both the micropores and mesopores. The decrease in condensate oil saturation in cores 1# and 2# were primarily attributed to the mesopores and macropores. The analysis suggests that as the core becomes tighter, it becomes more difficult for condensate oil to overcome the capillary resistance in the tiny throat of the dense core. Additionally, the adhesive oil film in the dense core has strong viscous forces, and the overall mobility of the pore fluid is restricted. As a result, the condensate oil saturation in core 3# remains high, and the condensate oil saturation in the micropores is always higher than in the mesopores and macropores (Sun and Guo, 2022).

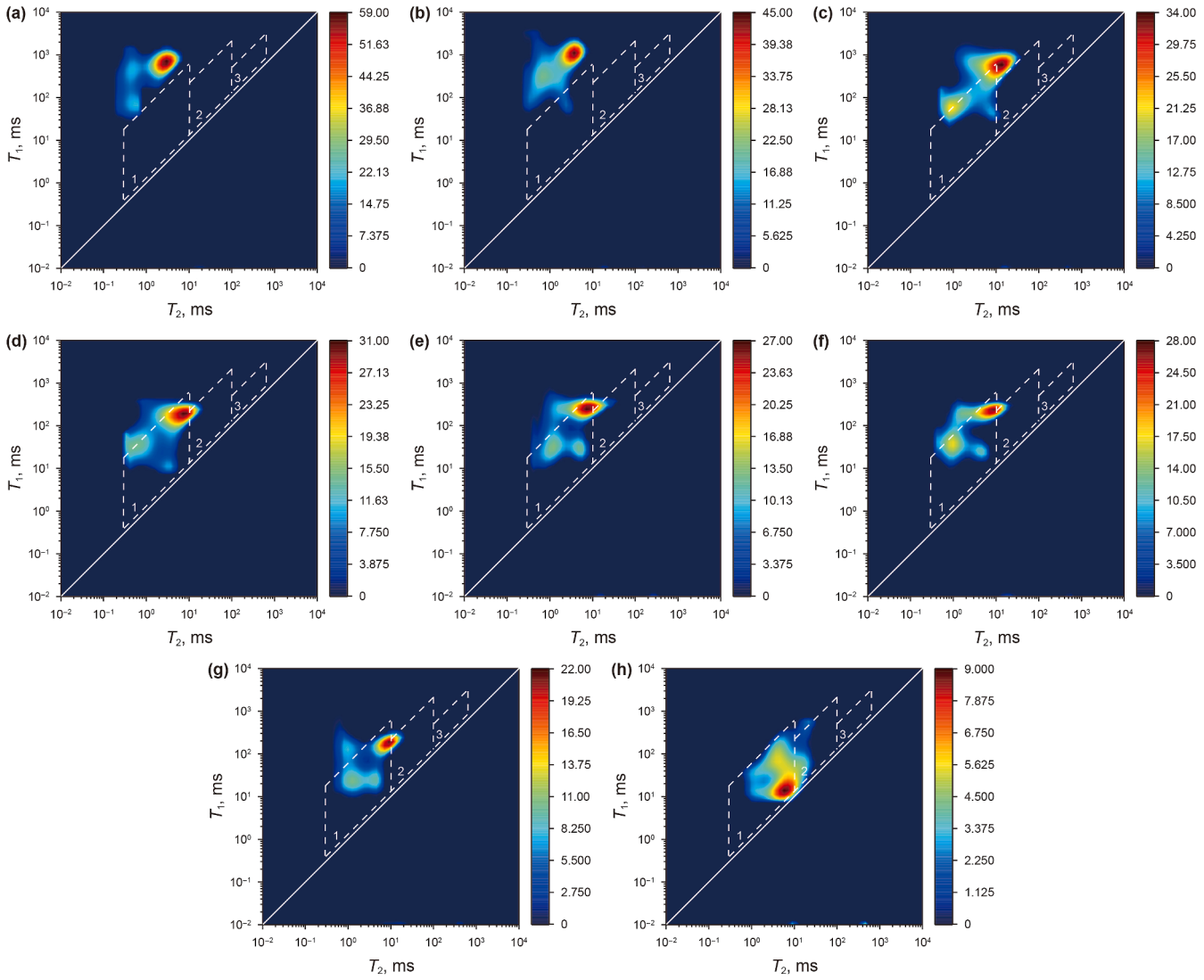

Fig. 9. The T_1–T_2 spectra describing the phase behavior of condensate gas with a CO_2 content of 4.78% in core 3#. (**a**)–(**h**) represent the signal distribution of condensate oil at pressures of 30.0, 27.1, 24.1, 21.1, 16.9, 11.9, 6.9, and 1.0 MPa, respectively. The white dashed rhombus frames indicate the calibrated signal range of condensate oil. The color scale on the right represents the hydrogen signal intensity at specified T_1 and T_2 coordinates.

Subsequently, comparing the results with the bulk PVT phase (Fig. 8), it is evident that the condensate oil saturation in the porous medium is lower than the values obtained from the bulk PVT phase. Due to the limitations of the PVT visualization cell, condensate liquid accumulates rapidly at the bottom during constant volume depletion, and the condensate oil at the bottom is not extracted as the pressure continues to deplete. In contrast, when the pressure drops below the dew point in the porous medium, some of the newly condensed condensate liquid exists in a dispersed state. Near the dew point, the interfacial tension is low, and the condensate oil exists in a critical suspended state as tiny molecular droplets that the gas phase can carry. At this point, the critical flow saturation is nearly 0, and the gas and oil phases appear to be miscible, with condensate oil being carried by the gas flow. Only a small amount of condensate oil remains on the walls. Additionally, during the depletion process, "liquid bridge" models may appear in the larger pore throats of the high permeability cores, with some condensate oil forming "liquid bridges" that are displaced from the porous medium. This phenomenon has also been observed in microfluidic experiments (Bian et al., 2019; Cheong et al., 2013; Hu et al., 2021; Jing et al., 2024b).

3.3. The impact of CO_2 content on the phase behavior of condensate gas

The extraction effect of CO_2 on the light hydrocarbon components in condensate gas significantly impacts the phase behavior

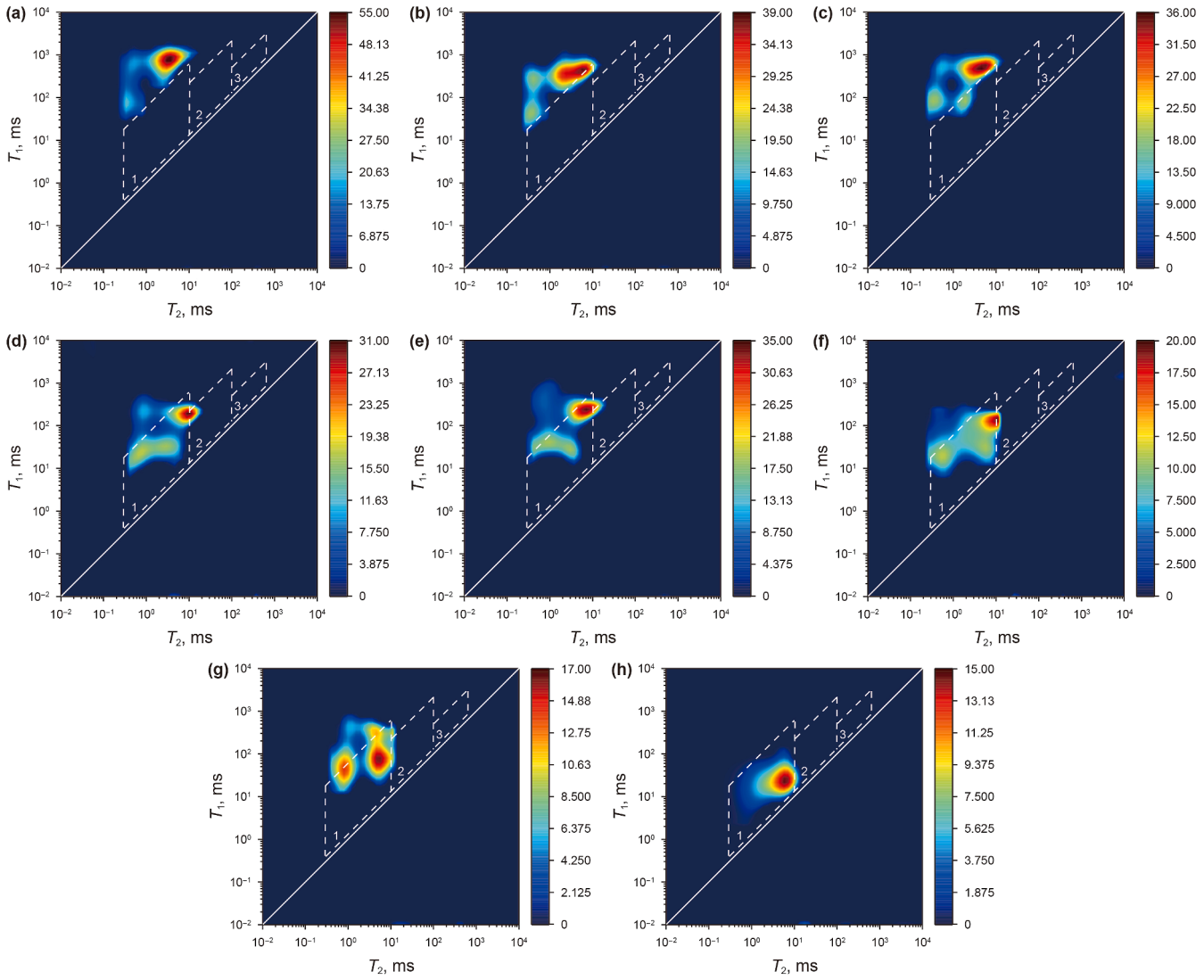

Fig. 10. The T_1–T_2 spectra describing the phase behavior of condensate gas with a CO_2 content of 9.56% in core 3#. (**a**)–(**h**) represent the signal distribution of condensate oil at pressures of 30.0, 26.4, 23.4, 20.4, 15.6, 10.0, 5.0, and 1.0 MPa, respectively. The white dashed rhombus frames indicate the calibrated signal range of condensate oil. The color scale on the right represents the hydrogen signal intensity at specified T_1 and T_2 coordinates.

of condensate gas (Chen et al., 2022; Zhang et al., 2020). Although conventional bulk PVT phase experiments have been extensively studied, the nanoconfinement effect caused by the porous medium in an actual reservoir needs to be detected using 2D NMR method to assess the impact of CO_2 on the phase behavior of condensate gas under nanoconfinement effects. The experiment uses 2D NMR T_1–T_2 spectral analysis to investigate the impact of CO_2 content (0, 4.78%, 9.56%, and 15.35%) on the phase behavior of condensate gas samples (Figs. 7 and 9–11). The saturation of condensate oil in different pore regions are shown in Figs. S4(c) and S5. The bulk PVT phase results are compared with the result of 2D NMR T_1–T_2 spectrum calculation (Fig. 12). The core sample used was core 3#. At a pressure of 30 MPa, the T_1/T_2 values of condensate gas with four different CO_2 contents are all higher than the T_1/T_2 recognition value for condensate oil, indicating that the condensate gas in the core is in a single gas phase. As the pore pressure began to deplete, condensate oil signals were first observed in the micropores, but the dew point pressures varied. As the CO_2 concentration increased, the dew point pressure negatively correlated with CO_2 concentration, with values of 27.9, 27.1, 26.4, and 24.7 MPa, respectively. This is attributed to CO_2's strong supercritical fluid extraction ability, which suppresses the retrograde condensation of condensate oil. Additionally, CO_2 and oil have competitive adsorption, which can strip different oil components (Liu et al., 2025a, Liu et al., 2025b; Yang et al., 2019; Zhang et al., 2020). The maximum retrograde condensation pressure also negatively correlated with CO_2 concentration, with values of 18.7, 16.9, 15.6, and 14.7 MPa, respectively.

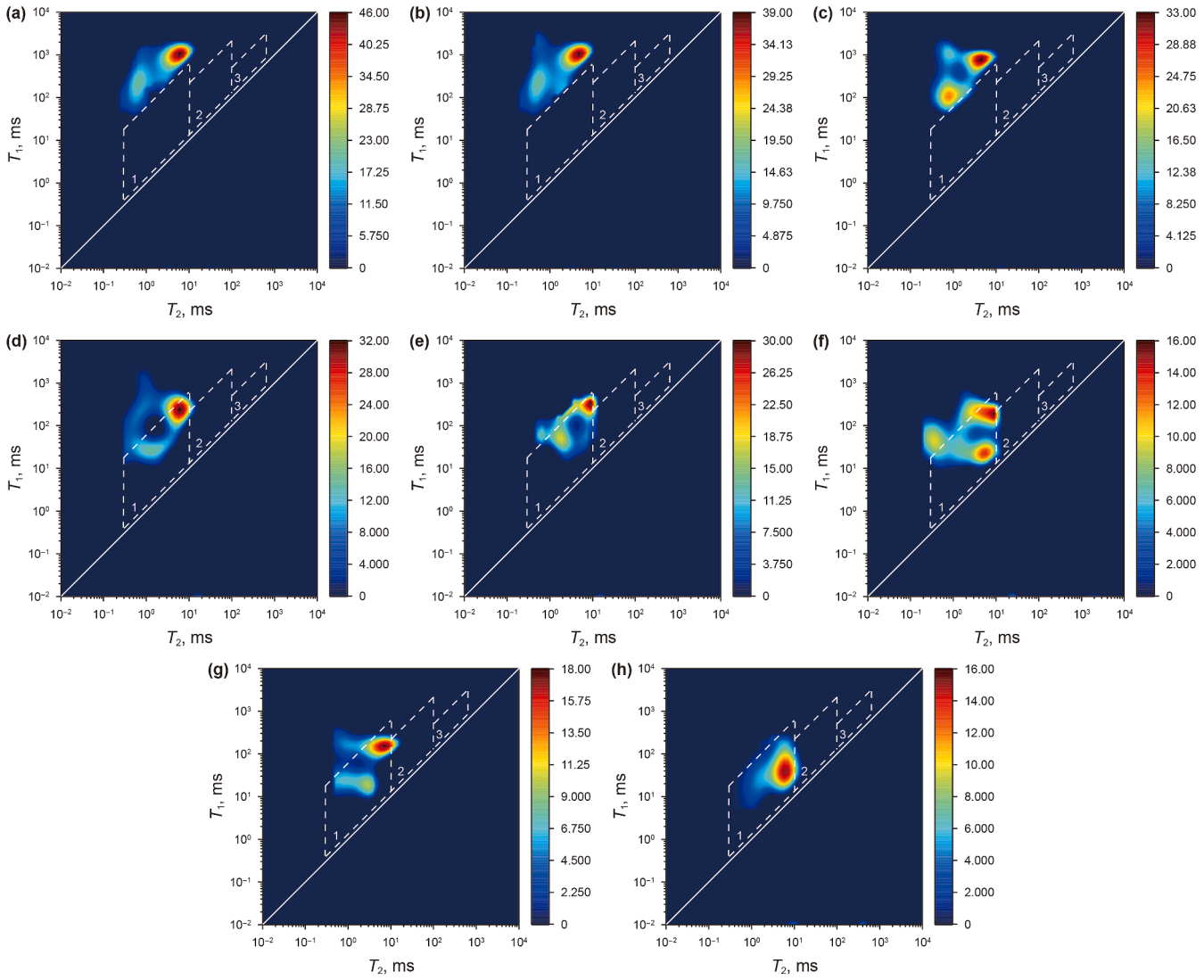

Fig. 11. The T_1–T_2 spectra describing the phase behavior of condensate gas with a CO_2 content of 15.35% in core 3#. (**a**)–(**h**) represent the signal distribution of condensate oil at pressures of 30.0, 28.0, 24.7, 19.7, 14.7, 9.7, 5.7, and 1.0 MPa, respectively. The white dashed rhombus frames indicate the calibrated signal range of condensate oil. The color scale on the right represents the hydrogen signal intensity at specified T_1 and T_2 coordinates.

From Figs. 9–11, it can be observed that as the pressure decreases, the condensate oil extracted from the condensate gas with the four CO_2 concentrations is mainly concentrated in the micropores, with a small amount of condensate oil signal appearing in the mesopores and almost no signal in the macropores. The maximum saturation of condensate oil in the micropores are 16.28%, 14.46%, 13.31%, and 11.87%, while the overall maximum retrograde condensation saturation is 17.35%, 15.56%, 14.28%, and 12.53%, respectively (Figs. S4(c) and S5). Condensate oil is predominantly concentrated in the micropores. This is because the micropores has a high specific surface area, and the heavier components tend to form oil films on the surface of the core particles, making the micropores critical in the condensation process (Liu C. et al., 2023; Liu S. et al., 2023).

A similar trend is observed in the bulk PVT phase (Fig. 12). In the experiments, the dew point pressures for condensate gas with four different CO_2 contents are found to be 25.16, 24.25, 23.30, and 22.32 MPa, respectively, which are all higher than the dew point pressures in the porous medium. Similarly, the condensate oil saturation in the bulk PVT phase is higher than the condensate oil saturation in the porous medium. The analysis suggests that the molecular movement rate is accelerated under the influence of nanoconfinement effects, making it more difficult for condensate gas to retrograde into the oil phase, resulting in a decrease in the heavy condensate oil saturation in the core (Jia et al., 2024; Wang S. et al., 2023).

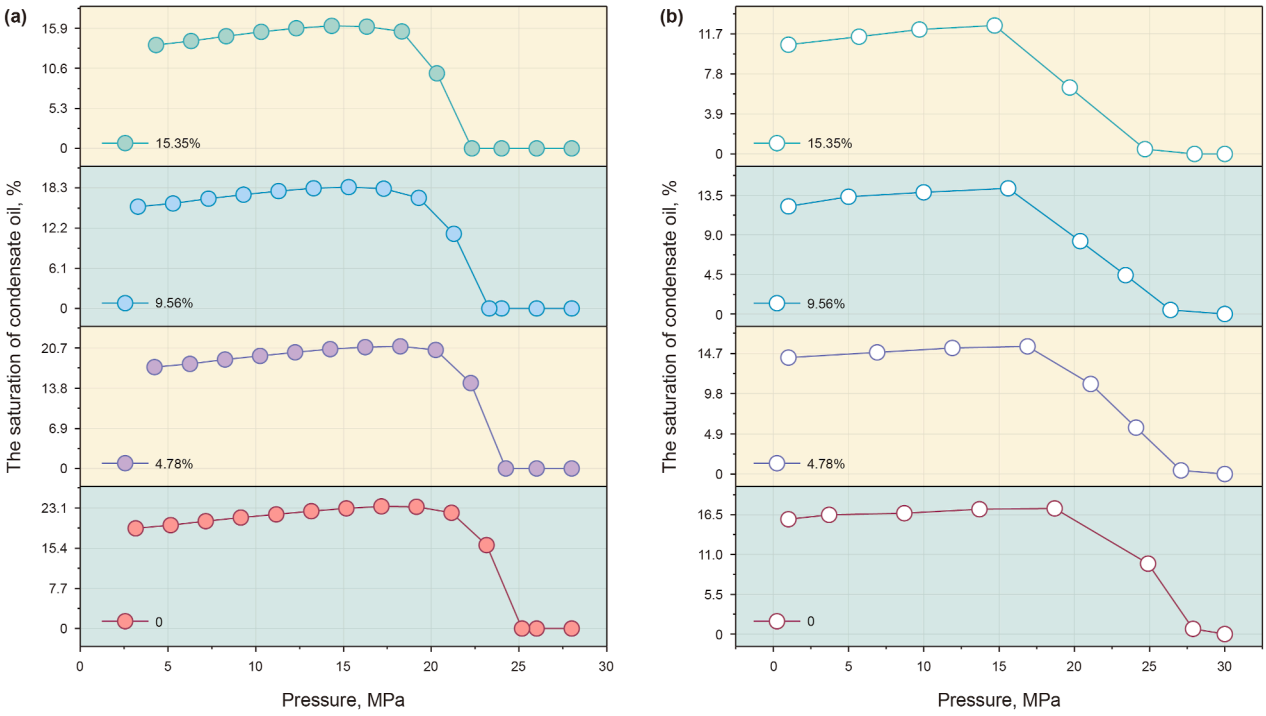

Fig. 12. The effect of CO_2 content on the saturation of condensate gas. The results were obtained from the PVT phase experiments (**a**) and the in-situ real time NMR scanning (**b**).

4. Conclusions

This study considers the influence of the nanoconfinement effect and quantitatively analyzes the phase behavior changes of condensate gas in nanoporous media. The experiment conducted in-situ real-time NMR scanning of condensate gas in cores 1#, 2#, and 3# to obtain 2D NMR T_1–T_2 spectra, investigating the effects of different cores and different CO_2 contents on the phase behavior of condensate gas. The study also compared the phase behavior of condensate gas in porous media with that in bulk PVT phase.

The retrograde condensation phenomenon first occurs in the micropores for any condensate gas system in porous media. As the tightness of the porous medium increases, the dew point pressure rises from 25.9 to 27.9 MPa, and condensate oil signals are detected in the mesopores and macropores in cores with lower density. The core's high density limits the flow of pore fluids, and as the density decreases, the maximum condensate oil saturation decreases from 17.35% to 10.35%. Compared with the bulk PVT phase experimental results, the dew point pressure of condensate gas in the porous medium is lower than that in the PVT visualization cell. This is due to the presence of porous media, which leads to oil–gas miscibility near the dew point and makes condensate oil in the macropore throats more easily displaced, forming “liquid bridges".

CO_2 content inhibits the retrograde condensation phenomenon in tight cores. As the CO_2 content increases, the dew point pressure of condensate gas in the core decreases from 27.9 to 24.7 MPa. The high specific surface area in the micropores makes it easier for heavy components to adsorb onto the surface, concentrating condensate oil signals in the micropores, where condensate oil dominates. The maximum condensate oil saturation in the micropores at different CO_2 concentrations was 17.35%, 15.56%, 14.28%, and 12.53%, respectively.

This study suggests that 2D NMR T_1–T_2 spectrum method is more suitable for quantitatively analyzing phase behavior changes and distribution patterns of condensate gas in porous media, providing strong evidence for analyzing fluid phase behavior characteristics in porous media. In future work, we will continue to study the different condensate gas components in porous media and the phase behavior characteristics of condensate gas under varying water saturation conditions.

CRediT authorship contribution statement

Yi-Sheng Hu: Writing – review & editing, Methodology, Conceptualization. **Heng Wang:** Writing – original draft, Investigation, Formal analysis. **Ping Guo:** Methodology, Conceptualization. **Yang Zhao:** Investigation.

Declaration of interests

The authors declare that they have no known competing financial interests or personal relationships that could have appeared to influence the work reported in this paper.

Acknowledgements

This research was financially supported by the National Science and Technology Major Project "Technology Demonstration for Efficient Development of Deep Buried-Hill Oil and Gas Fields in the Bohai Sea" (2024ZD1403803) and "Mechanistic Study of Gas Injection for Enhanced Oil Recovery in Offshore Sandstone Reservoirs" (2025ZD1402903).

Appendix A. Supplementary data

Supplementary data to this article can be found online at https://doi.org/10.1016/j.petsci.2025.11.007.

References

Alanazi, A., Baban, A., Ali, M., Keshavarz, A., Iglauer, S., Hoteit, H., 2023. Residual trapping of CO_2, N_2, and a CO_2-N_2 mixture in Indiana limestone using robust

NMR coreflooding: Implications for CO_2 geological storage. Fuel 353, 129221. https://doi.org/10.1016/j.fuel.2023.129221.
Aliyev, E., Saidian, M., Prasad, M., Russell, B., 2016. Rock typing of tight gas sands: A case study in Lance and Mesaverde formations from Jonah field. J. Nat. Gas Sci. Eng. 33, 1260–1270. https://doi.org/10.1016/j.jngse.2015.12.045.
Amani, M., Nguyen, N.T., 2015. An overview of methods to mitigate condensate banking in retrograde gas reservoirs. Adv. Petrol. Explor. Dev. 9 (2), 1–6. https://doi.org/10.3968/7023.
Arias-Ortiz, D., Patzek, T.W., 2025. Physics-based, data-driven production forecasting in the Utica and Point Pleasant Formation. Geoenergy Sci. Eng. 246, 213491. https://doi.org/10.1016/j.geoen.2024.213491.
Bian, X., Huang, H., Chen, L., 2019. Formation of special liquid bridges between a single plate and parallel plates. AIP Adv. 9 (9), 095018. https://doi.org/10.1063/1.5114684.
Chai, R., Liu, Y., Xue, L., Rui, Z., Zhao, R., Wang, J., 2022. Formation damage of sandstone geothermal reservoirs: During decreased salinity water injection. Appl. Energy 322, 119465. https://doi.org/10.1016/j.apenergy.2022.119465.
Chen, H., Liu, X., Zhang, C., Tan, X., Yang, R., Yang, S., et al., 2022. Effects of miscible degree and pore scale on seepage characteristics of unconventional reservoirs fluids due to supercritical CO_2 injection. Energy 239, 122287. https://doi.org/10.1016/j.energy.2021.122287.
Cheong, B.H.P., Lye, J.K.K., Backhous, S., Liew, O.W., Ng, T.W., 2013. Microplates based on liquid bridges between glass rods. J. Colloid Interface Sci. 397, 177–184. https://doi.org/10.1016/j.jcis.2013.01.043.
Dawaymeh, F., Ayoub, E., Khaleel, M., Alamoodi, N., 2025. Insights into the application of microfluidic platforms in enhanced oil recovery. Petroleum 11 (4), 422–439. https://doi.org/10.1016/j.petlm.2025.05.006.
Dianshi, X., Lehua, Z., Min, W., Rui, W., Xiaodie, G., 2024. The relationship between oiliness and mobility and their controlling factors for lacustrine shale oil: A case study of Qing1 member in Changling Sag, Songliao Basin. Fuel 376, 132738. https://doi.org/10.1016/j.fuel.2024.132738.
Dorhjie, D.B., Aminev, T., Gimazov, A., Khamidullin, D., Kuporosov, D., Maerle, K., et al., 2025. Impact of depletion rate on the thermodynamics of gas condensates: Experimental insights and analysis. Gas Sci. Eng. 134, 205534. https://doi.org/10.1016/j.jgsce.2024.205534.
Dorhjie, D.B., Aminev, T., Mukhina, E., Gimazov, A., Babin, V., Khamidullin, D., et al., 2024. The underlying mechanisms that influence the flow of gas-condensates in porous medium: A review. Gas Sci. Eng. 122, 205204. https://doi.org/10.1016/j.jgsce.2023.205204.
Gallego-Gómez, F., Morales, M., Blanco, A., López, C., 2018. Tunable visual detection of dew by bare artificial opals. Adv. Funct. Mater. 28 (21), 1800591. https://doi.org/10.1002/adfm.201800591.
Gu, M., Xie, R., Guo, J., Jin, G., 2023. Evaluation of fluid saturation in shale using 2D nuclear magnetic resonance. Energy Fuels 37 (4), 2713–2720. https://doi.org/10.1021/acs.energyfuels.2c03383.
Hassan, A., Mahmoud, M., Al-Majed, A., Elsayed, M., Al-Nakhli, A., BaTaweel, M., 2020. Performance analysis of thermochemical fluids in removing the gas condensate from different gas formations. J. Nat. Gas Sci. Eng. 78, 103333. https://doi.org/10.1016/j.jngse.2020.103333.
Hu, F., Zhou, C., Li, C., Xu, H., Zhou, F., Si, Z., 2012. Fluid identification method based on 2D diffusion-relaxation nuclear magnetic resonance (NMR). Petrol. Explor. Dev. 39 (5), 591–596. https://doi.org/10.1016/S1876-3804(12)60080-9.
Hu, H., Jiang, P., Huang, F., Xu, R., 2021. Role of trapped liquid in flow boiling inside micro-porous structures: Pore-scale visualization and heat transfer enhancement. Science Bulletin 66 (18), 1885–1894. https://doi.org/10.1016/j.scib.2021.05.019.
Jia, Z., Cao, R., Pu, B., Cheng, L., Li, P., Awotunde, A.A., et al., 2024. Effects of non-equilibrium phase behavior in nanopores on multi-component transport during CO_2 injection into shale oil reservoir. Energy 307, 132614. https://doi.org/10.1016/j.energy.2024.132614.
Jing, W.L., Zhang, L., Li, A.F., Zhong, J.J., Sun, H., Yang, Y.F., et al., 2024c. Phase behavior of gas condensate in porous media using real-time computed tomography scanning. Pet. Sci. 21 (2), 1032–1043. https://doi.org/10.1016/j.petsci.2023.11.009.
Jing, W., Zhang, L., Zhang, Y., Memon, B.S., Li, A., Zhong, J., et al., 2023. Phase behavior of gas condensate in fractured-vuggy porous media based on microfluidic technology and real-time computed tomography scanning. Phys. Fluids 35 (12), 122002. https://doi.org/10.1063/5.0175119.
Jing, W., Li, A., Zhou, S., Zhang, L., Zhong, J., Cui, S., et al., 2024a. Experimental study on the influence of fractured-vuggy porous media on condensate gas depletion production. Petrol. Sci. Technol. 42 (22), 3284–3300. https://doi.org/10.1080/10916466.2023.2195429.
Jing, W., Zhang, L., Li, A., Liu, T., Cheng, Y., Sun, H., et al., 2024b. Phase behaviors of gas condensate at pore scale: Direct visualization via microfluidics and in-situ CT scanning. SPE J. 29 (5), 2566–2577. https://doi.org/10.2118/218421-PA.
Kleinberg, R., Farooqui, S.A., Horsfield, M., 1993. T_1/T_2 ratio and frequency dependence of NMR relaxation in porous sedimentary rocks. J. Colloid Interface Sci. 158, 195–198. https://doi.org/10.1006/jcis.1993.1247.
Li, A., Zhang, Y., Zhang, K., Chen, X., Cheng, Y., Yang, X., et al., 2024. Effect of wax content on phase behavior of ultra-deep condensate gas reservoir: Experimental and thermodynamic model. Fuel 365, 131147. https://doi.org/10.1016/j.fuel.2024.131147.
Li, C., Tan, M., Li, C., Wang, K., Liu, P., Xiao, C., et al., 2024. Intelligent identification and quantitative evaluation method of fluid components from T_2-T_1 2D NMR logging. SPE J. 29 (10), 5426–5440. https://doi.org/10.2118/223091-PA.
Li, J., Huang, W., Lu, S., Wang, M., Chen, G., Tian, W., et al., 2018. Nuclear magnetic resonance T_1–T_2 map division method for hydrogen-bearing components in continental shale. Energy Fuels 32 (9), 9043–9054. https://doi.org/10.1021/acs.energyfuels.8b01541.
Li, J., Jiang, C., Wang, M., Lu, S., Chen, Z., Chen, G., et al., 2020. Adsorbed and free hydrocarbons in unconventional shale reservoir: A new insight from NMR T_1-T_2 maps. Mar. Petrol. Geol. 116, 104311. https://doi.org/10.1016/j.marpetgeo.2020.104311.
Li, J., Wang, M., Fei, J., Xu, L., Shao, H., Li, M., et al., 2022. Determination of in situ hydrocarbon contents in shale oil plays. Part 2: Two-dimensional nuclear magnetic resonance (2D NMR) as a potential approach to characterize preserved cores. Mar. Petrol. Geol. 145, 105890. https://doi.org/10.1016/j.marpetgeo.2022.105890.
Li, J., Zhao, G., Jia, X., Yuan, W., 2017. Integrated study of gas condensate reservoir characterization through pressure transient analysis. J. Nat. Gas Sci. Eng. 46, 160–171. https://doi.org/10.1016/j.jngse.2017.07.017.
Li, M., Wang, D., Shao, Z., 2020. Experimental study on changes of pore structure and mechanical properties of sandstone after high-temperature treatment using nuclear magnetic resonance. Eng. Geol. 275, 105739. https://doi.org/10.1016/j.enggeo.2020.105739.
Li, Q., Li, X., Zan, K., Song, Z., Shi, J., Wu, K., 2013. Experimental research of critical condensate saturation and flow characteristics of gas condensate reservoir. Petrol. Sci. Technol. 31 (13), 1361–1370. https://doi.org/10.1080/10916466.2010.543727.
Li, X., Ma, W., Zhang, Z., Chu, J., Song, Y., 2024. Low-field MRI study of the ^{1}H distribution and migration in porous sediments during natural gas conversion from methane hydrate. Geoenergy Sci. Eng. 243, 213397. https://doi.org/10.1016/j.geoen.2024.213397.
Liu, B., Jiang, X.W., Bai, L.H., Lu, R.S., 2022. Investigation of oil and water migrations in lacustrine oil shales using 20 MHz 2D NMR relaxometry techniques. Pet. Sci. 19 (3), 1007–1018. https://doi.org/10.1016/j.petsci.2021.10.011.
Liu, C., Sun, R., Zhao, J., Hu, Y., Mo, J., 2023. Enhancement of water collection efficiency by optimizing hole size and ratio of hydrophilic-superhydrophobic area on hybrid surfaces. J. Environ. Chem. Eng. 11 (5), 111082. https://doi.org/10.1016/j.jece.2023.111082.
Liu, S., Sun, H., Zhang, D., Yang, K., Li, X., Wang, D., et al., 2023. Experimental study of effect of liquid nitrogen cold soaking on coal pore structure and fractal characteristics. Energy 275, 127470. https://doi.org/10.1016/j.energy.2023.127470.
Liu, X., Chen, H., Chen, Z., Yang, R., Song, L., Bai, M., et al., 2024. Study on characterization and distribution of four regions of tight sandstone condensate gas reservoirs in the depletion development process. Fuel 358, 130267. https://doi.org/10.1016/j.fuel.2023.130267.
Liu, X., Chen, H., Cheng, W., Li, Y., Zhao, Y., Zhu, Y., et al., 2025a. Occurrence states and transport behavior of crude oil in different permeability oil reservoirs during depletion development. Geoenergy Sci. Eng. 252, 213944. https://doi.org/10.1016/j.geoen.2025.213944.
Liu, X., Chen, H., Li, Y., Zhu, Y., Liao, H., Zhao, Q., et al., 2025b. Oil production characteristics and CO_2 storage mechanisms of CO_2 flooding in ultra-low permeability sandstone oil reservoirs. Petrol. Explor. Dev. 52 (1), 196–207. https://doi.org/10.1016/S1876-3804(25)60014-0.
Liu, Y., Pan, Y., Xiong, Y., Sun, Y., Liang, B., Sun, L., 2025. Study on the mechanism of stress sensitivity and retrograde condensation coupling effect on reservoir depletion development in fractured-vuggy carbonate rocks. SPE J. 30 (1), 198–209. https://doi.org/10.2118/223941-PA.
Long, K., Tang, Y., He, Y., Luo, Y., Hong, Y., Sun, Y., et al., 2024. Full-cycle enhancing condensate recovery-underground gas storage by integrating cyclic gas flooding and storage from gas condensate reservoirs. Energy 293, 130724. https://doi.org/10.1016/j.energy.2024.130724.
Lu, Z., Ping, H., Chen, H., Zhang, Y., Xie, Z., Zhang, Y., et al., 2024. Geochemical characteristics of Ordovician crude oils in the FI17 strike-slip fault zone of the Fuman Oilfield, Tarim Basin: Implications for ultra-deep hydrocarbon accumulation in the Tarim basin. Mar. Petrol. Geol. 163, 106800. https://doi.org/10.1016/j.marpetgeo.2024.106800.
Luo, S., Chen, F., Zho, u D., Nasrabadi, H., 2021. Multiscale pressure/volume/temperature simulation of decreasing condensate/gas ratio at greater than dew-point pressure in shale gas-condensate reservoirs. SPE J. 26 (6), 4174–4186. https://doi.org/10.2118/203905-PA.
Meng, X., Sheng, J.J., 2016. Experimental and numerical study of huff-n-puff gas injection to re-vaporize liquid dropout in shale gas condensate reservoirs. J. Nat. Gas Sci. Eng. 35, 444–454. https://doi.org/10.1016/j.jngse.2016.09.002.
Rabiei, A., Sayyad, H., Riazi, M., Hashemi, A., 2015. Determination of dew point pressure in gas condensate reservoirs based on a hybrid neural genetic algorithm. Fluid Phase Equilib. 387, 38–49. https://doi.org/10.1016/j.fluid.2014.11.027.
Salahshoor, S., Fahes, M., 2020. Experimental determination of the dew point pressure for bulk and confined gas mixtures using an isochoric apparatus. Fluid Phase Equilib. 508, 112439. https://doi.org/10.1016/j.fluid.2019.112439.
Shi, J., Huang, L., Li, X., Sepehrnoori, K., 2015. Production forecasting of gas condensate well considering fluid phase behavior in the reservoir and wellbore. J. Nat. Gas Sci. Eng. 24, 279–290. https://doi.org/10.1016/j.jngse.2015.03.033.
Suleimanov, B.A., Suleymanov, A.A., Abbasov, E.M., Baspayev, E.T., 2018. A mechanism for generating the gas slippage effect near the dewpoint pressure in a porous media gas condensate flow. J. Nat. Gas Sci. Eng. 53, 237–248. https://doi.org/10.1016/j.jngse.2018.03.003.

Sun, B., Guo, P., 2022. The application of nuclear magnetic resonance 1D T_2 and 2D T_1–T_2 maps in the research of condensate oil saturation in condensate gas reservoirs. Energy Fuels 36 (14), 7581–7591. https://doi.org/10.1021/acs.energyfuels.2c01689.

Sun, C.Y., Liu, H., Yan, K.L., Ma, Q.L., Liu, B., Chen, G.J., et al., 2012. Experiments and modeling of volumetric properties and phase behavior for condensate gas under ultra-high-pressure conditions. Ind. Eng. Chem. Res. 51 (19), 6916–6925. https://doi.org/10.1021/ie2025757.

Tang, Y., Long, K., Wang, J., Xu, H., Wang, Y., He, Y., et al., 2021. Change of phase state during multi-cycle injection and production process of condensate gas reservoir based underground gas storage. Petrol. Explor. Dev. 48 (2), 395–406. https://doi.org/10.1016/S1876-3804(21)60031-9.

Tuo, H., Mensah, D.A., Chen, H., Abro, Z., Zhou, W., Ma, Y., et al., 2024. Phase behavior of the mid-deep carboniferous near critical condensate gas reservoir in Junggar Basin. China. Energy Fuels 38 (14), 12949–12959. https://doi.org/10.1021/acs.energyfuels.4c02054.

Wan, T., Mu, Z., 2018. The use of numerical simulation to investigate the enhanced Eagle Ford shale gas condensate well recovery using cyclic CO_2 injection method with nano-pore effect. Fuel 233, 123–132. https://doi.org/10.1016/j.fuel.2018.06.037.

Wang, J., Lu, S., Zhang, P., Li, Q., Yin, Y., Li, W., et al., 2024. Characterization of shale oil and water micro-occurrence based on a novel method for fluid identification by NMR T_2 spectrum. Fuel 374, 132426. https://doi.org/10.1016/j.fuel.2024.132426.

Wang, J., Zhang, P., Lu, S., Yin, Y., Wu, C., Yi, Y., et al., 2025. In situ fluid content evaluation of shale oil reservoirs: Insights from laboratory and wellsite mobile full-diameter core NMR. Nat. Resour. Res. https://doi.org/10.1007/s11053-025-10465-2.

Wang, P., Jia, Y., Zhong, J., Huang, W., Ding, W., Lian, P., et al., 2025. Study on the condensate gas phase behavior in Nano-porous media. Fuel 379, 132976. https://doi.org/10.1016/j.fuel.2024.132976.

Wang, S., Gu, Z., Guo, P., Zhao, W., 2024. Comparative laboratory wettability study of sandstone, tuff, and shale using 12-MHz NMR T_1-T_2 fluid typing: Insight of shale. SPE J. 29 (9), 4781–4803. https://doi.org/10.2118/221496-PA.

Wang, S., Zhang, H., Jin, B., Qiao, R., Wen, X.H., 2023. Molecular insights of condensate trapping mechanism in shale oil reservoirs and its implications on lean gas enhanced oil recovery. Chem. Eng. J. 476, 146366. https://doi.org/10.1016/j.cej.2023.146366.

Wang, X., Cui, B., Feng, Z., Shao, H., Huo, Q., Zhang, B., et al., 2023. In-situ hydrocarbon formation and accumulation mechanisms of micro- and nano-scale pore-fracture in Gulong shale, Songliao Basin, NE China. Petrol. Explor. Dev. 50 (6), 1269–1281. https://doi.org/10.1016/S1876-3804(24)60465-9.

Xu, C., Xie, R., Guo, J., Liu, J., 2024. Wettability and fluid characterization in shale based on T_1/T_2 variations in solvent extraction experiments. Fuel 355, 129512. https://doi.org/10.1016/j.fuel.2023.129512.

Yang, S., Wu, K., Xu, J., Li, J., Chen, Z., 2019. Roles of multicomponent adsorption and geomechanics in the development of an Eagle Ford shale condensate reservoir. Fuel 242, 710–718. https://doi.org/10.1016/j.fuel.2019.01.016.

Yao, Y., Wang, Z., Li, G., Wu, H., Wang, J., 2016. Potential of carbon dioxide miscible injections into the H-26 reservoir. J. Nat. Gas Sci. Eng. 34, 1085–1095. https://doi.org/10.1016/j.jngse.2016.07.073.

Zhang, A., Fan, Z., Zhao, L., 2020. An investigation on phase behaviors and displacement mechanisms of gas injection in gas condensate reservoir. Fuel 268, 117373. https://doi.org/10.1016/j.fuel.2020.117373.

Zhang, G., Chen, T., Wang, F., Sun, B., Wang, Y., Hou, D., 2021. Experimental determination of deviation factor of natural gas in natural gas reservoir with high CO_2 content. In: E3S Web Conf. EDP Sciences, vol. 245, 01045. https://doi.org/10.1051/e3sconf/202124501045.

Zhang, S., Wang, M., Zhu, X., Li, C., Cai, J., Yan, J., 2024. Oil saturation quantitative evaluation in lacustrine shale: Novel insights from NMR T_1-T_2 and displacement experiments. Fuel 371, 132062. https://doi.org/10.1016/j.fuel.2024.132062.

Zou, J., Hu, W., Lun, Z., Zhou, X., Zhao, C., Wang, H., et al., 2024. Recovery of adsorbed and free oil in shale formations by CO_2 injection: An experimental study using 1D- and 2D-NMR. Energy Fuels 38 (14), 12989–13001. https://doi.org/10.1021/acs.energyfuels.4c02207.